Structure and dynamics of nanofluids: Theory and simulations to calculate viscosity

Liudmila A. Pozhar
Department of Chemical and Process Engineering, University of Surrey, Guildford, Surrey, United Kingdom and Institute for Electromagnetic Research, Kharkov, Ukraine
(Received 28 June 1999)

The simplified expression of the Pozhar-Gubbins (PG) rigorous, nonequilibrium statistical mechanical theory of dense, strongly inhomogeneous fluids is used to calculate the viscosity of model fluids confined in a slit pore of several molecular diameters in width in terms of the *equilibrium* structure factors (i.e., the number density and pair correlation functions) of these nanofluids obtained by means of the equilibrium molecular dynamic simulations. These results are compared to those obtained by means of the nonequilibrium molecular dynamic simulations of the planar Poiseuille flow of the model nanofluids, and to the results supplied by several heuristic expressions for the nanofluid viscosity. This comparison proves that the PG transport theory provides a reliable, quantitatively accurate description of the viscosity coefficients of the model nanofluids while all the heauristic approaches fail. This success of the PG prediction of the nanofluid viscosity is because the theoretical expression accounts accurately for the nanofluid structure.

PACS number(s): 66.10.Cb, 02.10.Jf, 05.20.−y, 05.60.−k

I. INTRODUCTION

The nonequilibrium properties of strongly inhomogeneous fluids, such as those on interfaces and confined in narrow capillary pores of several molecular diameters in width (or nanopores) show a rich variety of behavior, including enhanced or inhibited viscosity, thermal conductivity and diffusion rates, modified phase transitions, highly selective adsorption, etc. Understanding of these properties is very important both for fundamental and applied research as almost any natural or industrial process involves transport phenomena in nanofluids. Examples include adsorption, catalysis, separation, lubrication, drying, wetting, living cells metabolism, flows in disordered media and many other processes. Progress in nanomaterials and device development concentrates on the use of atomic and molecular clusters, i.e., nanofluids on interfaces and quantum nanofluids in atomic traps, that will shape the future technologies, in spite of difficulties experienced by experimental studies of such systems at present.

Elaborate engineering [1] and experimental studies of nanofluids confined in nanopores started in the beginning of the 60s with pioneering works by Mysels *et al.* [2] and Derjaguin *et al.* [3] Accumulating experimental evidence [4] triggered further molecular simulations and heuristic theoretical studies of the transport properties of nanofluids [5,6]. This resulted in the first microscopic theory of nonequilibrium phenomena in inhomogeneous fluids suggested by Davis [7] at the end of the 1980s. Davis's approach relies on the Enskog-like kinetic equation for the dense hard sphere fluid modified by incorporation of long-range attractive interactions in a mean-field sense, and the assumption that the nonequilibrium state of the inhomogeneous fluid is locally equilibrium. The pair correlation function of the inhomogeneous fluid is assumed to be that of the corresponding homogeneous fluid at some local set of the fluid densities as approximated by the Fischer-Methfessel functional of the density distribution. The Davis expressions for the transport coefficients cover several particular cases of simple pore geometry and depend upon flow types. These spatially dependent coefficients are further averaged to obtain the corresponding effective, scalar transport coefficients.

Though Davis's theory has been in a good qualitative agreement with known experimental and NEMD data, it suffers from several major shortcomings. In particular, the theory does not describe nanofluids on interfaces and in confinements of other than simple slit or cylindrical geometry. The derived expressions for the transport coefficients are not general, and therefore, cannot be applied to any nanofluids other than those considered in the case studies. Finally, Davis's transport coefficients do not include contributions caused by the interactions between fluid molecules and those of the confinement. These shortcomings of the Davis theory lead to large uncertainities in evaluation of the transport coefficients of nanofluids. In the following sections of this paper we demonstrate numerically that the details of the actual fluid-fluid and fluid-surface correlations make a great impact on the local and average nanofluid viscosity even in the case of very simple, model nanofluids.

Over the last decade Pozhar and Gubbins (PG) have developed a rigorous statistical mechanical approach [8] to nonequilibrium phenomena in strongly inhomogeneous fluids that remains tractable, overcomes all the shortcomings of the Davis theory, and does not involve any assumptions about the density and structure of the fluids or geometry and structure of the confinements/interfaces. It relies on the rigorous generalization [9] of the Mori-Zwanzig projection operator technique [or the functional perturbation theory (FTP)] developed in the framework of the theory of dynamical systems. This new perturbation theory concerns derivation of the generalized Langevin equations (GLEs) to the desirable order of FPT (the nth order GLE has been derived). The order of a particular GLE depends upon an application. Such GLEs can be further used to derive kinetic and transport theories of systems of interest. This program has been realized for the most general case of strongly inhomogeneous fluids and has led to the corresponding generalized kinetic and quasihydrodynamic theories of strongly inhomogeneous

fluids. The derived explicit expressions for the generalized, nonlocal transport coefficients reveal extreme sensitivity of these coefficients to the structure factors of the fluids in the confinements and interfaces. The initial evaluation of the PG-theoretical viscosity has proved that it agrees within 5% with the NEMD-based data [10].

Recent technical improvements in the NEMD-computation technique led to reevaluation of some known data [11] on the velocity profile of the Poiseuille flow of nanofluids in narrow capillary pores of less than 10 molecular diameters σ in width. This revealed failure of known heuristic and MD simulation-based expressions for viscosities [11] and algorithms for such calculations [12] inherent from the methods developed for homogeneous or weakly inhomogeneous fluids. It has also become completely obvious that the NEMD simulations technique by itself is not capable of supplying a reasonable extension of the standard, bulk fluid viscosity definition applicable to nanofluids in such narrow pores [11].

In this paper we continue numerical evaluation of the PG-theoretical transport coefficients of nanofluids concentrating on the viscosity. Theoretical calculations of the PG-viscosity of nanofluids involve the fluid and wall molecule number densities and contact values of the fluid-fluid and fluid-wall pair correlation functions. These quantities are calculated in Sec. II for model nanofluids confined in a pore of 5.1σ of Refs. [10,11] using the EMD technique. In the course of these calculations we pay special attention to angular dependence of the contact values of the pair correlation functions. These data are further used to calculate major contributions to the PG-theoretical viscosity of the nanofluids so that the surface and fluid structure contributions are properly accounted for. The results confirm sensitivity of the nanofluid viscosity to the surface and fluid structure details. In Sec. III we describe NEMD-simulation data for the model fluids obtained using the fifth order Gear predictor-corrector method and examine thoroughly known heuristic expressions and possible new candidates for the NEMD''experimental'' viscosity of the nanofluids in the case of the Poiseuille flow. This examination proves that all of such heuristic, simplified expressions for the viscosity of nanofluids fail badly in all the studied cases leading to physically meaningless results (one of such cases was considered in Ref. [11]). The discussion in Sec. III shows that this failure is because such simplified expressions do not account properly for details of the fluid and surface structure via the corresponding pair correlation functions. In contrast, the PG-theoretical viscosity proves to be not only physically meaningful, but also a numerically accurate characteristic of the nanofluid flows.

II. THEORETICAL BACKGROUND

The PG transport theory concerns inhomogeneous fluids (including nanofluids) of nonreactive, structureless molecules on interfaces or in confinements (walls) composed of nonreactive, structureless molecules that cause the inhomogeneity of the nanofluids. The fluid-fluid and fluid-wall intermolecular interactions are assumed to be pairwise additive, central and decomposable into the sum

$$\phi(\mathbf{r}_{ij}) = \phi_H(\mathbf{r}_{ij}) + \phi_S(\mathbf{r}_{ij}) \tag{2.1}$$

of a hardcore repulsive contribution $\phi_H(\mathbf{r}_{ij})$,

$$\phi_H(\mathbf{r}_{ij}) = \begin{cases} +\infty, & \mathbf{r}_{ij} < \sigma, \\ 0, & \mathbf{r}_{ij} \geqslant \sigma, \end{cases} \tag{2.2}$$

and an attractive, continuous soft interaction, $\phi_S(\mathbf{r}_{ij})$, where $\mathbf{r}_{ij} = \mathbf{r}_i - \mathbf{r}_j$, and $\mathbf{r}_i$, $\mathbf{r}_j$ denote coordinate vectors assigned to the centers of interacting molecules i and j, respectively. The only requirement to the soft intermolecular interaction potential is that it should converge to zero faster than $1/|\mathbf{r}_{ij}|^2$ when $|\mathbf{r}_{ij}| \to \infty$($|\ |$ denotes the absolute value of $\mathbf{r}_{ij}$). The decomposition (2.1) of the actual intermolecular interaction can always be realized by means of the Barker-Henderson (BH) [13] or Weeks-Chandler-Andersen (WCA) [14] methods that supply the corresponding effective diameters of the hardcore intermolecular interactions σ_{BH} and σ_{WCA}, respectively. In the particular case of a nanofluid confined in a narrow slit pore with the inhomogeneity in the z direction (that is orthogonal to the wall planes) the simplified major terms in the general expression (3.34) of the first paper in Ref. [8] for the PG-theoretical viscosity of strongly inhomogeneous fluids reduce to the formula

$$\eta_{\mathrm{slit}}(z) = \eta\{4\pi n^*(z)\tau_\eta^*(z)[1+\pi\beta^{*0}(z)]^2 + (16/5)\pi n^*(z)\beta^{*0}(z)\}, \tag{2.3}$$

where $\eta = (5/16\sigma^2)(m/\pi\beta)^{1/2}$ is the viscosity of a dilute hard sphere gas, $\beta = 1/(k_B T)$, k_B is the Boltzmann constant, T denotes temperature, m is the mass of a fluid molecule, σ denotes the hardcore diameter of the fluid molecules specific to the fluid-fluid hardcore intermolecular interactions, $n^*(z) = n(z)\sigma^3$ is the dimensionless equilibrium number density, $n(z)$, of the nanofluid, and other quantities are as follows. The dimensionless quantity $\tau_\eta^*(z)$,

$$\tau_\eta^*(z) = \{2\pi[\nu^*(z) + (1/3)\nu_1^*(z) + \sqrt{2}\,\nu_2^*(z)]\}^{-1}, \tag{2.4}$$

is proportional to the visco relaxation time and incorporates two essentially ''fluid'' contributions $\nu^*(z)$ and $\nu_1^*(z)$,

$$\nu^*(z) = \int_0^\pi d\theta \sin\theta n^*(z - \sigma\cos\theta) g(z, z - \sigma\cos\theta), \tag{2.5}$$

$$\nu_1^*(z) = \int_0^\pi d\theta \sin\theta [n^*(z - \sigma\cos\theta) - n^*(z)] \times g(z, z - \sigma\cos\theta), \tag{2.6}$$

and the contribution $\nu_2^*(z)$ due to fluid-wall intermolecular interactions

$$\nu_2^*(z) = \int_0^\pi d\theta \sin\theta n_w^*(z - \sigma_{fw}\cos\theta) g_{fw}(z, z - \sigma_{fw}\cos\theta), \tag{2.7}$$

where $g(z, z - \sigma\cos\theta)$ is the contact value of the equilibrium, fluid-fluid pair correlation function, θ is the angle between the vector connecting the centers of mass of the interacting molecules, $\mathbf{r}_{ij}$, and the positive z direction, $n_w^*(z)$

TABLE I. Units of the MD simulations quantities.

Quantity	Units
Number density, n	σ^3
Velocity, $\mathbf{u}$	$(\epsilon/m)^{1/2}$
Viscosity, η	$\sigma^{-2}(\epsilon m)^{1/2}$
Temperature, T	ϵ
Shear rate, γ	$\sigma^{-1}(\epsilon/m)^{1/2}$
Shear stress and pressure, $\mathbf{P}$	ϵ/σ^3
a	σ
b	σ

$=n_w(z)\sigma^3$ is the equilibrium, reduced number density of the wall molecules, $g_{fw}(z,z-\sigma_{fw}\cos\theta)$ is the contact value of the equilibrium, fluid-wall pair correlation function, and σ_{fw} is the hardcore diameter specific to the fluid-wall hardcore intermolecular interactions. The quantity $\beta^{*0}(z)$ is also defined in terms of the contact values of the equilibrium fluid-fluid pair correlation function and reduced number density

$$\beta^{*0}(z)=\int_0^{\pi} d\theta \sin^3\theta\cos^2\theta n^*(z-\sigma\cos\theta) \times g(z,z-\sigma\cos\theta). \tag{2.8}$$

In what follows we omit the asterisk, assuming that all quantities are reduced (see Table I).

There have been several assumptions used in deriving Eq. (2.3) for the simplified version of the PG slit pore nanofluid viscosity from the general expression (3.34) of the first paper in Ref. [8]. In particular, (i) those terms that are proportional to tensors composed of antisymmetric combinations of the direction cosine vector $\hat{\boldsymbol{\sigma}}$ have been neglected as they are not expected to contribute significantly to the viscosity of the studied model nanofluids (see discussion in Sec. IV of the first paper in Ref. [8]). Further, there has been (ii) a neglect of dependence of the contact values of the pair correlation functions upon the in-plane angle ψ of the polar coordinate system with the polar axes z used in Eqs. (2.3)–(2.8). Both of these assumptions may not be applicable to ''real'' nanofluids, and if such is the case, the general expressions, Eq. (3.34) of the first paper and Eq. (3.24) of the second paper in Ref. [8] (the case of nanofluid mixtures), should be used.

In this paper we use Eq. (2.3) for the PG viscosity of a nanofluid in a slit pore to calculate the viscosity of two model nanofluids confined in structured slit pores where fluid-fluid and fluid-wall intermolecular interactions are both modelled either (I) with the WCA repulsive potential (the WCA system),

$$\phi_{\mathrm{WCA}}(r)=\begin{cases} 4\epsilon\left[\left(\dfrac{\sigma}{r}\right)^{12}-\left(\dfrac{\sigma}{r}\right)^{6}\right]+\epsilon, & r<2^{1/6}\sigma, \\ 0, & r\geqslant 2^{1/6}\sigma, \end{cases} \tag{2.9}$$

or (II) with the Lennard-Jones (LJ) potential (the LJ system),

$$\phi_{\mathrm{LJ}}(r)=4\epsilon\left[\left(\frac{\sigma}{r}\right)^{12}-\left(\frac{\sigma}{r}\right)^{6}\right], \quad r>0, \tag{2.10}$$

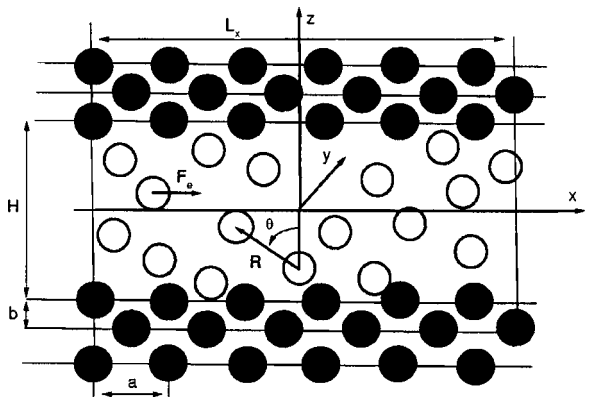

FIG. 1. Slit pore geometry used in the EMD and NEMD simulations.

where r denotes the absolute value of the coordinate vector between the centers of the interacting molecules, σ is the effective molecular diameter, and ϵ denotes the depth of the potential well.

The viscosity coefficient of Eq. (2.3) can be easily calculated provided the equilibrium, reduced fluid and wall number densities, the equilibrium pair correlation function values and the hardcore diameters are known for the composite potentials of Eq. (2.1) corresponding to the actual potentials of Eqs. (2.9) and (2.10).

III. EQUILIBRIUM MD SIMULATION TECHNIQUE

The equilibrium structure factors involved in Eq. (2.3) can be obtained from (i) integral equations of equilibrium statistical mechanics (see, for example, Ref. [16], and references therein), (ii) experimental data, and (iii) EMD simulations. In this study we used the EMD simulation method to recover the number densities and pair correlation function contact values of the model WCA and LJ nanofluids. In the course of this simulation the reduced potential parameters of the fluid-fluid and fluid-wall intermolecular interactions and molecular masses m were set equal to unity, $\epsilon=\sigma=m=1$. The model nanofluids (composed of $N_f=360$ fluid atoms in each case) were confined between parallel walls composed of immobile, structureless and nonreactive atoms of the atomic mass equal to unity. The pore width H was set equal to 5.1σ and was defined as the distance between the two parallel planes through the centers of the surface layers of wall atoms (see Fig. 1). Each wall consisted of three layers of atoms arranged in the fcc lattice structure of 72 atoms per layer totalling to $N_w=216$ atoms. Due to immobility of the wall molecules there was the momentum production in the systems that led to the excess heat production. This heat was removed from the fluids by the temperature scaling procedure [15]. The pore geometry and the model WCA fluid were chosen to mimic the simulation conditions of Refs. [10,11] so that our results could be easily compared to those obtained previously.

The reduced molecular dynamic (MD) simulation parameters are summarized in Table II for both model fluids. The MD simulations were performed for two different average fluid number densities defined as in Refs. [10,11],

$$n_{\mathrm{av}}^{f}=N_f/V_f, \tag{3.1}$$

TABLE II. Reduced parameters of the MD simulations.

Simulation box sizes		Pore width,	Fluid av. number	Wall av. number	Temperature	Parameter	Parameter
L	$L_x=L_y$	H	density, n_{av}^f	density, n_{av}^w	T	a	b
7.81	12.6373	5.1	0.442	0.85	0.729	2.2977	0.6775
8.7975	10.8195	5.1	0.603	0.85	0.958	1.9672	0.9244

where N_f is the number of fluid atoms in the ''roughly'' calculated volume V_f of the pore occupied by the fluid, $V_f = HL_xL_y$. This definition of the average fluid density was chosen for convenience of comparison of our simulation results with those of Ref. [10]. Actual average fluid densities are larger than the ''rough'' ones due to the fact that the 72 wall atoms framing the pore space on each side in z direction occupy some of the pore space. The average wall density is defined as

$$n_{\mathrm{av}}^w = N_w / V_w , \tag{3.2}$$

where N_w is the number of wall molecules and $V_w = bL_xL_y + \pi\sigma^3 N_w/18$ is the wall volume calculated with regard to the adopted wall geometry, Fig. 1. This definition of the wall volume V_w seems more appropriate than that of Ref. [10] as it does not include the pore space between wall atoms of the surface layers. This modified definition of the wall volume accounts for the difference in numerical values of the wall parameters a and b listed in Table II and those of Ref. [10] specific to the same average wall density.

For the MD simulations we used a fifth order Gear predictor-corrector algorithm with the reduced time step $t=0.008$. In the case of the EMD simulations of nanofluid structure properties this algorithm leads to reliable and physically meaningful results while other known algorithms (e.g., Verlet's leapfrog algorithm [15]) are not accurate enough to supply realistic values of such properties (see discussion in Sec. V). The periodic boundary conditions were applied in all three directions. The need to use the periodic boundary condition in the z direction was due to the fact that separation of the wall atoms was large enough for fluid molecules to penetrate beyond the wall surface layers. The first 50 000 EMD time steps were discarded and followed by further 3 950 000 of the EMD time steps. The equilibrium number density profiles were calculated by dividing the width of the pore in bins, $\Delta z = 5.1\times 10^{-2}$, and accumulating histograms of the numbers of molecules N_i in each bin.

The EMD calculation of the fluid-fluid and fluid-wall pair correlation function contact values $g_{ff}(z, z-\sigma\cos\theta)$ and $g_{fw}(z, z-\sigma\cos\theta)$, respectively, required an assumption concerning the maximal distance between the molecular centers at which the molecules could be considered in contact. This distance was set equal to $\sigma+\Delta R$ [where $\Delta R = \Delta z/500$], or $1.000102\sigma_d$, where σ_d denotes a hardcore diameter specific to the hardcore potential of Eqs. (2.1), (2.2). While both the WCA and BH hardcore diameters could be used, we chose the BH hardcore diameter σ_{BH} that does not depend upon the number density and is defined by the expression [13]

$$\sigma_{\mathrm{BH}} = \int_0^{r_m} dz\{1-\exp[-\beta\phi(z)]\}, \tag{3.3}$$

where $r_m = 2^{1/6}\sigma$ and $\phi(z)$ is the WCA potential of Eq. (2.9) or the LJ potential of Eq. (2.10). The WCA hardcore diameter is not an attractive choice in the case of nanofluids as it depends upon the nanofluid density and therefore, upon a position within the pore. Due to our choice of the parameters of the model intermolecular interaction potentials for the WCA and LJ systems we have for our systems $\sigma = \sigma_{fw} = \sigma_{\mathrm{LJ}} = \sigma_{\mathrm{BH}} = \sigma_{\mathrm{WCA}}$.

The fluid-fluid pair correlation function values specific to molecular contact were calculated using the histogram method and accuracy considerations discussed in Ref. [10],

$$g_{ij}(z, z-\sigma\cos\theta) = 2\langle N_{ij}\rangle / [n_i(z) n_j(z-\sigma\cos\theta) V_i V_j], \tag{3.4}$$

where V_i is the volume of the bin centered at z and containing the center of the molecule i, V_j is the volume occupied by the bin containing collision partners j of the molecule i at the polar angles between θ and $\theta+\Delta\theta$,

$$V_j = \pi\sigma^2\left[2+3\frac{\Delta R}{\sigma}+\left(\frac{\Delta R}{\sigma}\right)^2\right][\cos\theta-\cos(\theta+\Delta\theta)]\Delta R, \tag{3.5}$$

$\Delta\theta = \pi/50$ denotes the width of a θ bin, $\langle N_{ij}\rangle$ is the average number of such pairs of molecules i with their centers in the bin z and molecules j with their centers in the volume V_j, and $n_i(z)$ and $n_j(z-\sigma\cos\theta)$ denote the values of the fluid number density corresponding to the bins centered at z and $z-\sigma\cos\theta$, respectively. For our choice of $\Delta z, \Delta\theta$ and ΔR the volume V_j was less than 5×10^{-5}, and therefore, to keep the statistical error of the calculations of the pair correlation function contact values within 20% we performed the EMD simulations for four million time steps.

The fluid-wall pair correlation function contact values were calculated using Eqs. (3.4) and (3.5) where in this case the index i referred to a fluid molecule, the index j to a wall molecule, $\langle N_{ij}\rangle$ denoted the average number of pairs of contacting molecules, and the number density $n_j(z-\sigma\cos\theta)$ was that of the wall molecules. This number density was set to be equal to $6m/[\pi\sigma^3]$, $m=1$, within the actual space occupied by wall molecules and to zero everywhere else in the walls.

All integrals in Eqs. (2.5)–(2.8) were computed summing up the numerical values of the corresponding integral kernels and also using the composite trapezoid rule [17]. The results coincided to the fourth digit after the comma.

The contact values of the fluid-fluid and fluid-wall pair correlation functions specific to the model WCA and LJ nanofluid systems obtained by means of the above EMD technique are visualized in Figs. 2–9. At the same number densities and temperatures motion of the LJ fluid molecules

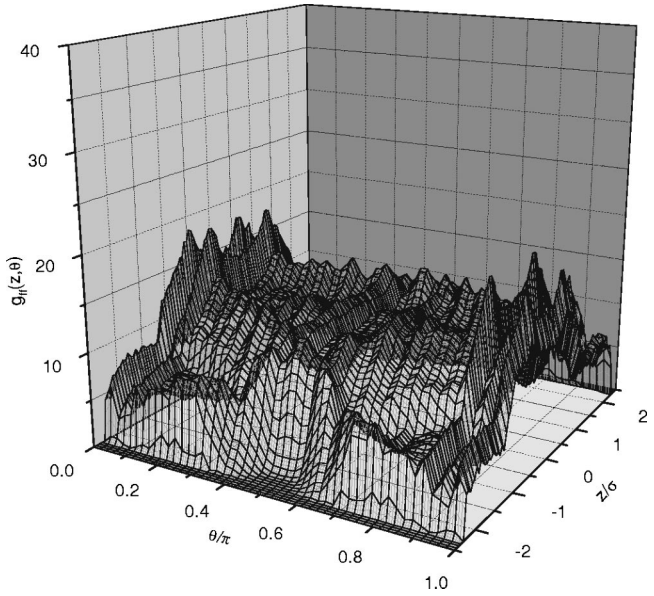

FIG. 2. The EMD contact values of the fluid-fluid pair correlation function for the model WCA nanofluid after 4 million time steps for $n_{\mathrm{av}}^{f}=0.442$ and $T=0.729$.

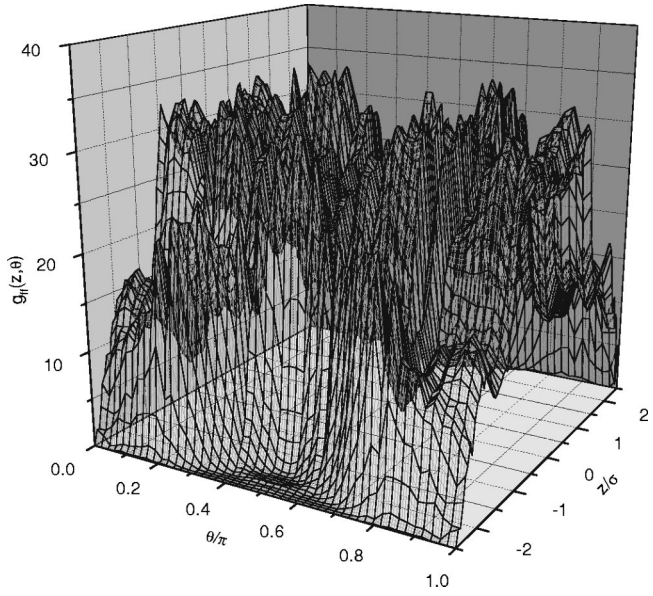

FIG. 4. The EMD contact values of the fluid-fluid pair correlation function for the model WCA nanofluid after 4 million time steps for $n_{\mathrm{av}}^{f}=0.603$ and $T=0.958$.

is more correlated than that of the WCA fluid molecules due to the presence of the attractive interactions. In both cases the excluded volume effects and the attractive interactions in the case of the LJ fluid lead to the number of preferential positions of the contacting molecules that manifest themselves via local maxima of the pair correlation function contact values. The difference in the structure of the two model fluids is enhanced near the pore walls for both densities. These data confirm our results and those obtained in numerous EMD studies of the pore nanofluid density, that the structure of nanopore fluids differs markedly from that of the corresponding bulk fluids.

For both model fluids the fluid-wall correlations are enhanced at large densities when more fluid molecules are forced to enter the available pore space between wall atoms of the wall surface layers. This phenomenon is reflected by a significant decrease in width and magnitude of the picks located about the positions ($z=-2.10$ to -2.35, $\theta/\pi=1.0$ to 0.9) in the case of the first wall and the positions ($z=2.10$ to 2.35, $\theta/\pi=0.0$ to 0.1) in the case of the second wall, and a simultaneous significant increase in the width and magnitude of the picks located at the positions ($z=-1.5$ to -2.55, $\theta/\pi=1.0$ to 0.5) and ($z=1.5$ to 2.55, $\theta/\pi=0$ to 0.5) (see Figs. 3, 5 and Figs. 7, 9, respectively). The presence of the attractive interactions in the model LJ systems does not affect significantly the positions of the picks with respect to those in the case of the model WCA system, but the magnitude of the picks grows for the LJ system.

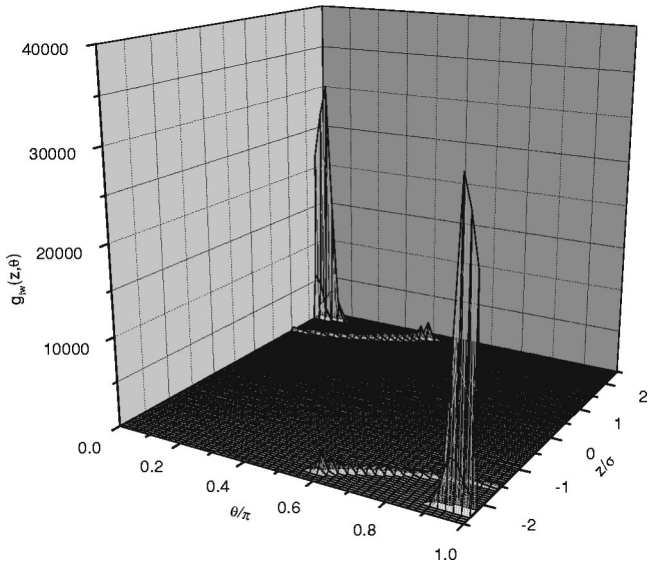

FIG. 3. The EMD contact values of the fluid-wall pair correlation function for the model WCA nanofluid after 4 million time steps for $n_{\mathrm{av}}^{f}=0.442$ and $T=0.729$.

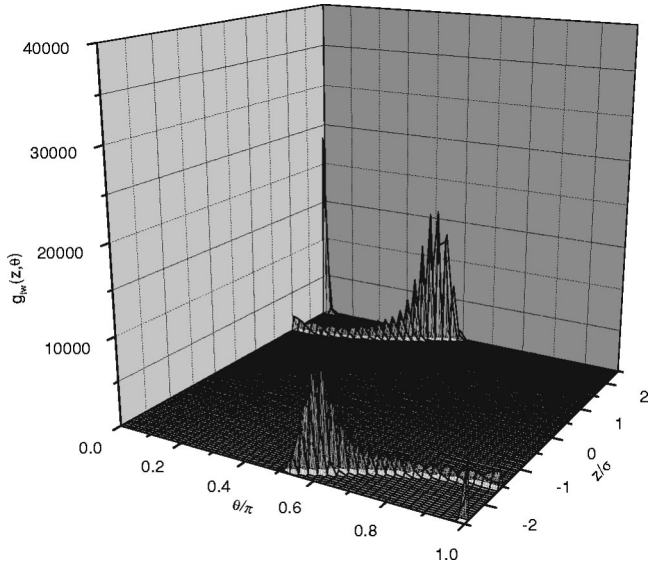

FIG. 5. The EMD contact values of the fluid-wall pair correlation function for the model WCA nanofluid after 4 million time steps for $n_{\mathrm{av}}^{f}=0.603$ and $T=0.958$.

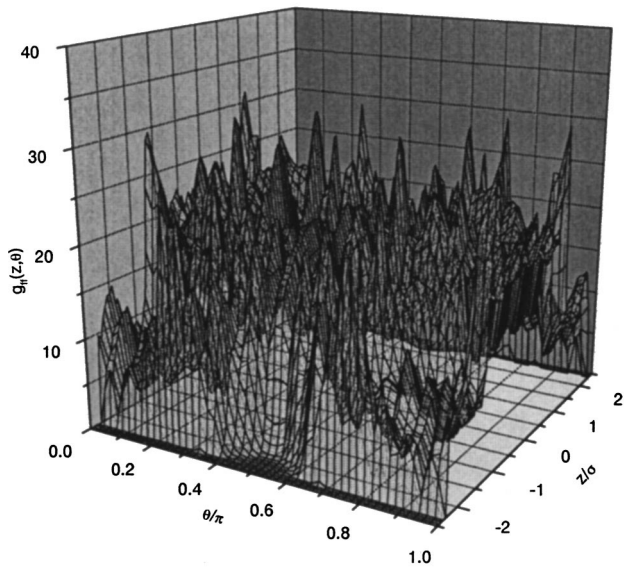

FIG. 6. The EMD contact values of the fluid-fluid pair correlation function for the model LJ nanofluid after 4 million time steps for $n_{\mathrm{av}}^{f}=0.442$ and $T=0.729$.

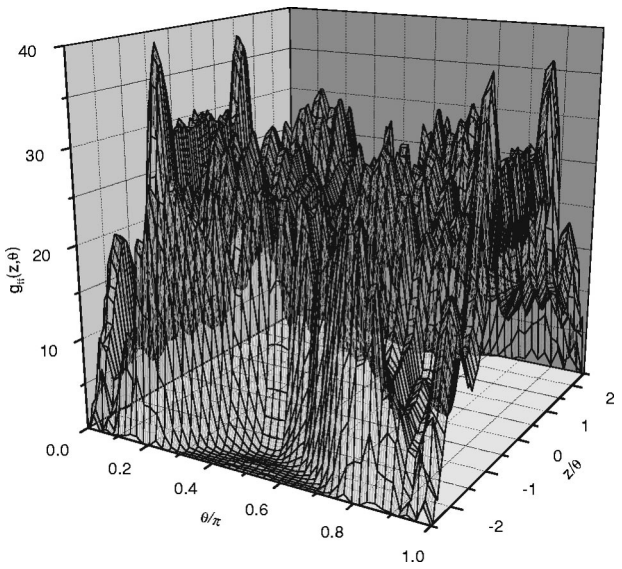

FIG. 8. The EMD contact values of the fluid-fluid pair correlation function for the model LJ nanofluid after 4 million time steps for $n_{\mathrm{av}}^{f}=0.603$ and $T=0.958$.

IV. NONEQUILIBRIUM MD SIMULATION TECHNIQUE

For bulk fluids the NEMD simulation method is an alternative, ''experimental'' route for calculation of the transport coefficients. It essentially involves the standard definition of the local tensorial viscosity $\boldsymbol{\eta}(\mathbf{r})$ of bulk fluids via the local tensorial shear stress $\mathbf{P}(\mathbf{r})$ and local tensorial strain rate $\boldsymbol{\gamma}(\mathbf{r})$,

$$\mathbf{P}(\mathbf{r})=\boldsymbol{\eta}(\mathbf{r}):\gamma(\mathbf{r}), \tag{4.1}$$

where a colon denotes the double inner product of the fourth rank tensor $\boldsymbol{\eta}(\mathbf{r})$ and the second rank tensor $\boldsymbol{\gamma}(\mathbf{r})$. For laminar flows of bulk fluids the viscosity tensor in Eq. (4.1) does not depend on a position.

In addition to the EMD simulations we performend the NEMD simulations of the Poiseuille flow of the WCA and LJ fluids of Sec. III. This flow was caused by the force F_e acting on each molecule in the x direction (see Fig. 1) and was thought to mimic a gravity flow of a simple nanofluid in a nanopore with atomistic walls [10,11]. The simulations were again performed using the fifth order Gear predictor-corrector algorithm to obtain the density and streaming velocity profiles. The width of the pore was divided in 500 z bins, and the value of the force was set equal to 0.02 in the units of ϵ/σ. Other simulation parameters were the same as those used in the EMD simulations. There are several other algorithms available for the NEMD simulations of transport properties of fluids one of which, so-called IMC algorithm developed in the first paper of Ref. [12], was used in previous works [10,11] for the NEMD simulations of the Poiseuille flow of nanofluids. However, the IMC algorithm in-

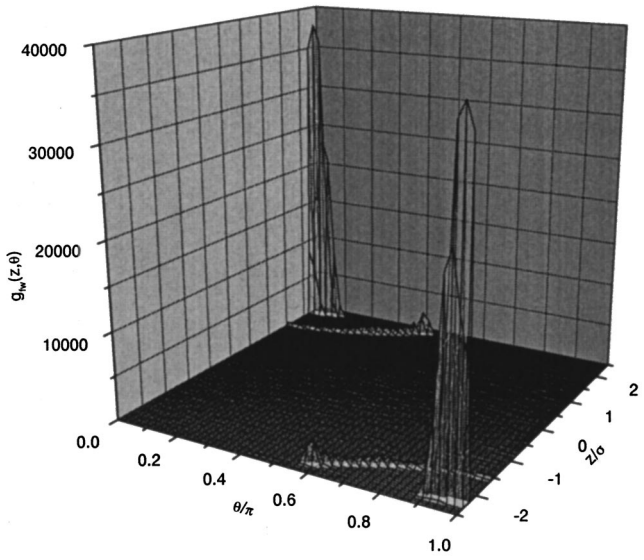

FIG. 7. The EMD contact values of the fluid-wall pair correlation function for the model LJ nanofluid after 4 million time steps for $n_{\mathrm{av}}^{f}=0.442$ and $T=0.729$.

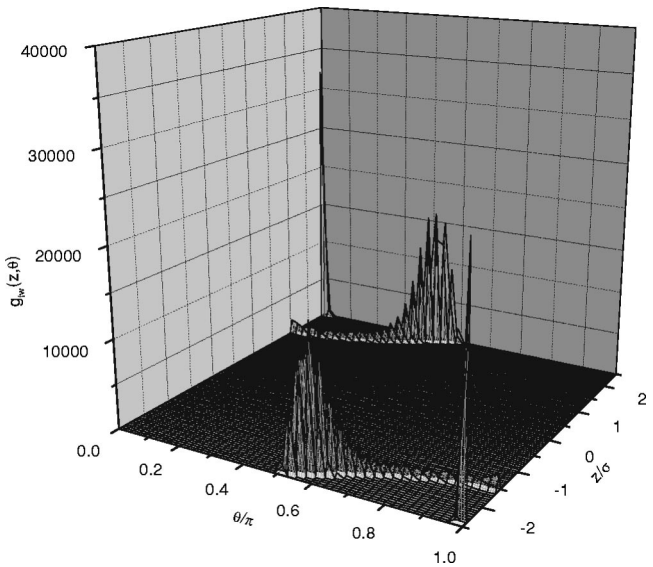

FIG. 9. The EMD contact values of the fluid-wall pair correlation function for the model LJ nanofluid after 4 million time steps for $n_{\mathrm{av}}^{f}=0.603$ and $T=0.958$.

cludes implicit assumptions that reduce its applicability to the systems of low fluid density and/or low potential field gradients. From analysis of the results obtained in this study and in previous works [10,11,18] (see Sec. V) it follows that the use of the IMC algorithm in the case of nanofluids leads to unrealistic, ''oversmoothed'' velocity profiles [10,11,18] of the Poiseuille flow and the underestimated NEMD viscosity coefficients.

For the physical systems and the MD simulation technique used in our simulations Eq. (4.1) leads to the explicit expression for the standard scalar local viscosity of the bulk fluid,

$$\eta_{\mathrm{NEMD}}(z)=-\lim_{F_e\to 0}\left\{\frac{\langle P_{xz}(z)\rangle}{\gamma(z)}\right\}, \tag{4.2}$$

where $P_{xz}(z)$ is the xz component of the shear stress tensor, $\langle\cdots\rangle$ means the time average that substitutes the ensemble average by virtue of the ergodicity theorem,

$$\gamma(z)=\frac{\partial u_x(z)}{\partial z} \tag{4.3}$$

is the only nonzero component of the strain rate tensor, and $u_x(z)$ is the x component of the streaming velocity of the nanofluid. In general, the viscosity of Eq. (4.2) does not depend on the position z for the laminar flow and can be easily calculated provided the quantities $\langle P_{xz}(z)\rangle$ and $\gamma(z)$ are known, for example, from the NEMD simulations. In the IMC method the average momentum flux is approximated by the position-dependent expression $\langle P_{xz}(z)\rangle=F_e\int_0^z dz'\rho(z')$, and therefore, from Eq. (4.2) it follows that for $F_e\to 0$ the IMC viscosity for our systems is

$$\eta_{\mathrm{IMC}}(z)=-F_e\int_0^z dz'\rho(z')\Big/\frac{\partial u_x(z)}{\partial z}. \tag{4.4}$$

From previous studies [11] and our results (see discussion in Sec. V) it is known that Eq. (4.4) leads to unphysical (divergent and negative) values of the viscosity due to large deviations of the velocity profile from the parabolic form that lead to strong oscillations of $\gamma(z)$. A pore-average substitute for $\eta_{\mathrm{IMC}}(z)$ can be provided in the case when the total momentum flux through the pore cross section is used in Eq. (4.4) and the velocity profile is roughly approximated by the parabolic one (see the first paper in Ref. [12]), $u_x(z)=c_2z^2+c_0$, where the coefficients c_2 and c_0 are obtained from the mean-square fit of the NEMD velocity profile by the parabolic one. For the pore geometry considered in our study this leads to the following expression for the pore average viscosity $\eta_{p\text{-av}}$,

$$\eta_{p\text{-av}}(z)=-F_e\int_{-H/2}^{H/2}dz'\rho(z')/[2Hc_2]. \tag{4.5}$$

From the results of our study it follows (Sec. V) that $\eta_{p\text{-av}}$ supplies much underestimated but still physically meaningful evaluation of the pore nanofluid viscosity ''from beneath.''

Another physically meaningful evaluation of the average pore viscosity can be obtained from Eq. (4.5) if, instead of the parabolic fit, the linear velocity profile fit is chosen so as $u_x(z=\pm H/2)=0$ and the maximal value of $u_x(z)$ is equal to that in the pore center $u_z(0)$,

$$\eta_{\mathrm{total}}(z)=F_eH\int_{-H/2}^{H/2}dz'\rho(z')/\{4[u_x(0)-u_x(-H/2)]\}. \tag{4.6}$$

This evaluation means that the pore viscosity is roughly equated to that of the pore Couette flow caused by dragging the thin layer of the pore fluid in the pore center in the x direction. As we discuss in Sec. V, this evaluation supplies relatively reasonable values of the average pore viscosity that for medium dense nanofluids can be used as a good evaluation ''from above.''

Other possible candidates for the ''coarse-grained'' pore viscosity can be suggested upon consideration of the physical nature of the process of the momentum redistribution in the system. The major contribution to this process comes from hard-core collisions over the ''minimal collision surface'' of direct molecular contact. In the case of spherical molecules this surface is a sphere of the radius equal to the hardcore diameter σ of the molecules. This consideration can be deducted from explicit expressions for transport coefficients of fluids obtained both in classical kinetic theories (see, for example, Ref. [19], and references therein) and in the PG theory [see, for example, Eq. (3.34) of the first paper in Ref. [8]]. This observation together with the considerations that led to Eq. (4.4) and approximation of the strain rate by the corresponding finite differences supply the following heuristic quantities:

$$\eta_{\sigma}(z)=2F_e\sigma\int_{-\sigma}^{\sigma}dz'\rho(z+z')/[u_x(z+\sigma)-u_x(z-\sigma)], \tag{4.7}$$

$$\eta_{\sigma/2}(z)=F_e\sigma\int_{-\sigma/2}^{\sigma/2}dz'\rho(z+z')/[u_x(z+\sigma/2)-u_x(z-\sigma/2)]. \tag{4.8}$$

From our NEMD results described in Sec. V it follows that these quantities may lead to meaningful (though poor) values of the pore viscosity far from the pore center and to divergencies in the pore center, due to the symmetry of the flow geometry.

A ''local'' substitute $\eta_{\mathrm{IMC}\,f}(z)$ for the IMC viscosity of Eq. (4.4) can be supplied if the partial derivative of the streaming velocity in this equation is substituted by the corresponding finite difference

$$\eta_{\mathrm{IMC}\,f}(z)=-F_eH\int_0^z dz'\rho(z')/\{2[u_x(z)-u_x(0)]\}. \tag{4.9}$$

Once again, our NEMD results discussed in Sec. V prove that this quantity supplies unphysical values of the pore viscosity.

Failure of all the above bulk-fluid based and heuristic approximations of the average and ''local'' pore viscosity is discussed in Sec. V. The physical meaning of this failure is that none of these approximations account accurately for the

nanofluid structure properties described by the fluid-fluid and fluid-wall correlation functions. In contrast to these heuristic quantities, the PG theoretical expression (2.3) incorporates the details of the nanofluid and wall structure via the pair correlation function contact values and therefore, leads to physically meaningful and numerically reasonable values of the pore viscosity for all the considered nanofluid systems.

Finally, in fluid mechanics the shear stress specific to the turbulent flows can be sometimes approximated as a functional of the nonlocal turbulent viscosity and the strain rate. For the system geometry used in this study such an approximation takes the form [11]

$$P_{xz}(z) = -\int_0^z dz'\,\eta(z;z-z')\,\gamma(z'). \qquad (4.10)$$

The reasons supporting this approximation are provided by the nonlocal nature of the turbulent vortices that define the type of flow and simplicity of such an approximation. In the case of nanofluids confined in nanopores and at interfaces of several molecular diameters in width turbulent vortices cannot exist, and therefore, there is no physical reason to expect the approximation (4.10) to be physically meaningful. The results of this study and that of the previous work [10] prove that the nonlocal nature of the nanofluid viscosity is properly accounted for in the PG theoretical expressions. In these expressions the seemingly local values assigned to the nanofluid viscosity at the position **r** are calculated in terms of integrals of the structure factors of the nanofluids over the sphere of the radius σ centered at the position **r**, and therefore, are essentially nonlocal. Physical meaning of this integration is that the transport coefficients represent collective response of the system to a disturbance and therefore, emerge as a consequence of redistribution of the mass, momentum and energy in the system via the molecular collision mechanism. A minimal number of such collisions is required for the system to respond to the disturbance, and this is represented by the integration over the ''minimal collision surface.'' This is yet another friutful realization of the collective mode description of many-particle system dynamics that supplies convenience of the ''coarse-grained,'' or quasicontinual, representation of the system transport properties.

V. RESULTS AND DISCUSSION

A. EMD simulations: the PG theoretical viscosities and nanofluid structure

In addition to the contact values of the pair correlation functions, calculation of the PG theoretical viscosity of Eq. (2.3) requires data on the fluid number density. In our EMD simulations we recovered the number density profiles of the model nanofluids and used this data together with the data on the contact values of the pair correlation functions to calculate the integrals of Eqs. (2.6)–(2.8) and the PG theoretical viscosity. The final results obtained after 4 million EMD time steps for the model WCA systems are shown on Figs. 10 and 11, and for the model LJ systems on Figs. 12 and 13. For both types of the model nanofluids the density profiles reflect the fact that fluid molecules can penetrate between the wall atoms of the surface layers. This phenomenon becomes more prominent at the high average density and temperature

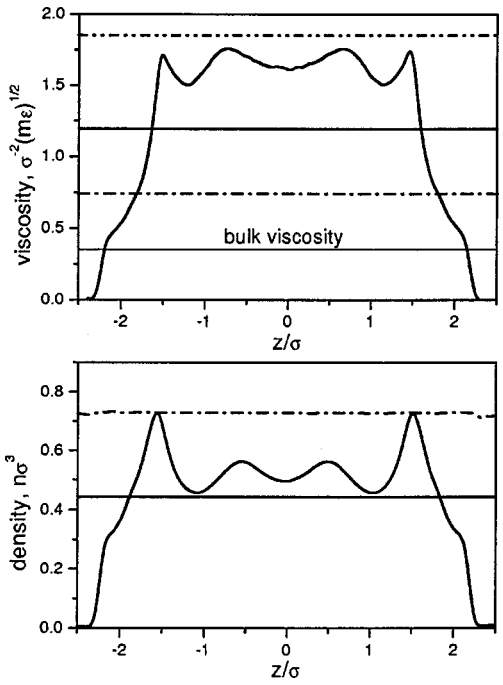

FIG. 10. The PG-theoretical viscosity $\eta_{\rm slit}$ and density profiles (solid curves) of the model WCA nanofluid after 4 million EMD time steps for $n^f_{\rm av}=0.442$ and $T=0.729$. Straight lines in the top figure: (1) —, the average PG-theoretical viscosity, $\eta^{\rm av}_{\rm slit}=1.193$; (2) -··-, $\eta_{\rm total}=1.851$; (3) -·-, $\eta_{p\text{-}{\rm av}}=0.739$, $c_2=0.00608$; the bulk viscosity is equal to 0.350. Straight lines in the bottom figure: (1) —, $n^f_{\rm av}$; -·-, temperature profile. Parameters: m, molecular mass; ε,σ potential parameters.

($n^f_{\rm av}=0.603, T=0.958$). In the case of the model LJ nanofluids the presence of attractive interactions manifests itself in that the density profiles become more structured, their maxima higher and minima deeper than those in the case of the model WCA nanofluids at the corresponding average densities and temperatures. This confirms an intuitive expectation that in addition to the excluded volume effects the attractive interactions supply a powerful mechanism for effective layering of the nanofluid molecules. Within the LJ nanofluid layers near the walls the number density can be twice as large as the corresponding average one (see, for example, Fig. 12). In the case of the model WCA systems fluid layers are less prominent at the pore center than those of the model LJ fluids at the corresponding average densities.

The most striking result of our calculation is that the average PG-theoretical viscosity of all the model nanofluids exceeds that of the WCA bulk fluid at the corresponding densities and temperatures by a factor from 3 to 4 (the WCA fluid viscosity is the largest possible bulk fluid viscosity at a given fluid type, density and temperature). These findings correlate with well-known experimental data on the viscosity of ''real'' nanofluids [4,20]. Although these experimental data were obtained for nanofluids composed of complicated molecules, and therefore, cannot be compared directly with those obtained in our study, the average PG theoretical viscosity of the model nanofluids reflects the major tendency of the experimental viscosity towards a significant increase (up to 4 times) in its value compared to that of the corresponding bulk fluids. In this respect our new data differ from those obtained in the previous work [10] where the Verlet's leap-

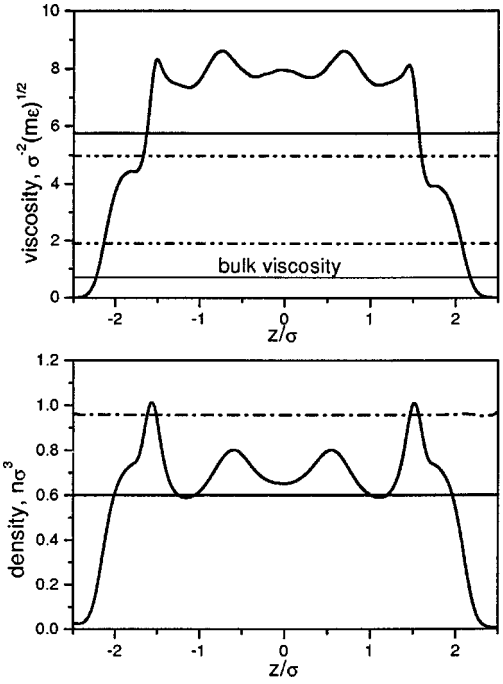

FIG. 11. The PG-theoretical viscosity, η_{slit}, and density profiles (solid curves) of the model WCA nanofluid after 4 million EMD time steps for $n^f_{\text{av}}=0.603$ and $T=0.958$. Straight lines in the top figure: (1) —, the average PG-theoretical viscosity, $\eta^{\text{av}}_{\text{slit}}=5.762$; (2) -···-, $\eta_{\text{total}}=4.966$; (3) -··-, $\eta_{p\text{-av}}=1.900$, $c_2=0.00317$; the bulk viscosity is equal to 0.700. Straight lines in the bottom figure: (1) —, n^f_{av}; -··-, temperature profile. Parameters: m, molecular mass; ε,σ, potential parameters.

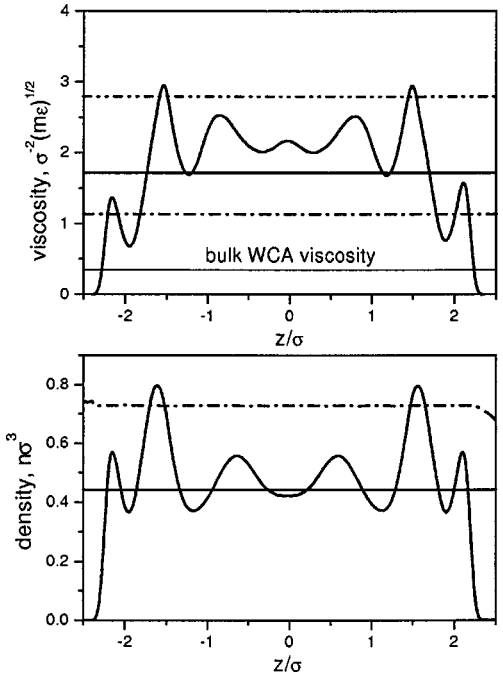

FIG. 12. The PG-theoretical viscosity, η_{slit}, and density profiles (solid curves) of the model LJ nanofluid after 4 million EMD time steps for $n^f_{\text{av}}=0.442$ and $T=0.729$. Straight lines in the top figure: (1) —, the average PG-theoretical viscosity, $\eta^{\text{av}}_{\text{slit}}=1.716$; (2) -···-, $\eta_{\text{total}}=2.798$; (3) -··-, $\eta_{p\text{-av}}=1.136$, $c_2=0.0039$; the WCA bulk viscosity is equal to 0.350. Straight lines in the bottom figure: (1) —, n^f_{av}; -··-, temperature profile. Parameters: m, molecular mass; ε,σ, potential parameters.

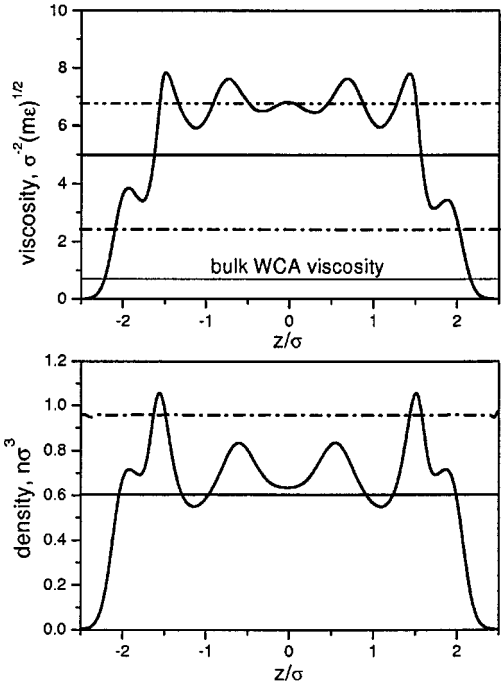

FIG. 13. The PG-theoretical viscosity, η_{slit}, and density profiles (solid curves) of the model LJ nanofluid after 4 million EMD time steps for $n^f_{\text{av}}=0.603$ and $T=0.958$. Straight lines in the top figure: (1) —, the average PG-theoretical viscosity, $\eta^{\text{av}}_{\text{slit}}=4.983$; (2) -···-, $\eta_{\text{total}}=6.764$; (3) -··-, $\eta_{p\text{-av}}=2.415$, $c_2=0.00252$; the WCA bulk viscosity is equal to 0.700. Straight lines in the bottom figure: (1) —, n^f_{av}; -··-, temperature profile. Parameters: m, molecular mass; ε,σ, potential parameters.

frog algorithm, too wide z bins and large volumes V_{ij} allowed for the contacting molecule pairs led to ''smoothing'' the contact values of the pair correlation functions, and therefore, to largely underestimated values of the nanofluid viscosity. The integral expressions of Eqs. (2.6)–(2.8) are very sensitive to the shape of the correlation functions. This shape can be easily oversmoothed when too large volumes V_{ij} are assumed as the molecular contact volume. From our recent computer experiments we found that the optimal V_{ij} value should be set from 10^{-4} to 10^{-5}. If this value is larger than 10^{-3} the calculated correlation functions do not reflect properly local order in nanofluids. At the V_{ij} values lower than 10^{-5} statistical errors become very large and simulation time increases by the order of magnitude.

The complex, layered structure of the model nanofluids leads to significant increase in the ''local'' nanofluid viscosity reflected by Eq. (2.3) via the integral contributions of the fluid number density and contact values of the pair correlation functions, Eqs. (2.6)–(2.8). Although the viscosity profile carries effects of strong density variations over the fluid layers, the magnitude of its oscillations is low. In the ''free'' pore space where there are no wall atoms (i.e., at the distances larger than $\sigma/2$ from the walls) the magnitude of the viscosity profile oscillations is largest in the case of the model LJ fluid at the lower average density, but it does not exceed 20% of the viscosity value in the pore center. The magnitude of such oscillations in the case of the model WCA fluid and for the denser LJ fluid does not exceed 10% of the corresponding viscosity values in the pore center. This reflects complicated consequences of the ordering role of the

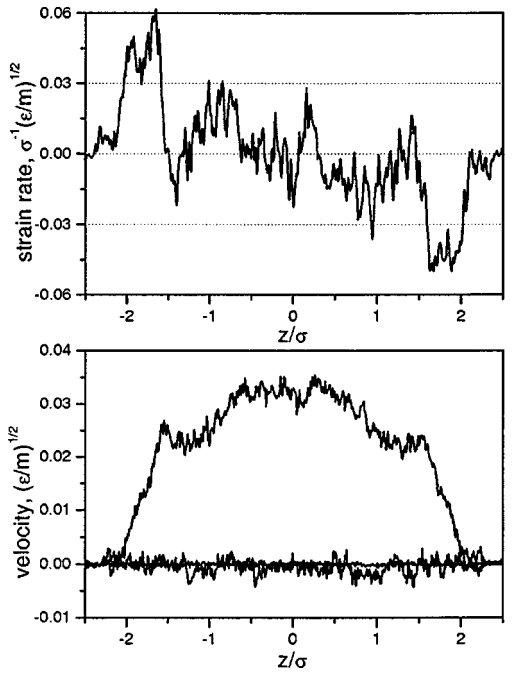

FIG. 14. The model WCA nanofluid: the NEMD velocity (bottom) and strain rate, $\partial u_x(z)/\partial z$, (top) profiles after 1 million EMD time steps for $n_{\mathrm{av}}^f=0.442$ and $T=0.729$. The bottom figure: the developed profile, $u_x(z)$; the two fluctuating lines parallel to the coordinate axis: low fluctuations, $u_y(z)$; large fluctuations, $u_z(z)$. Parameters: m, molecular mass; ε,σ, potential parameters.

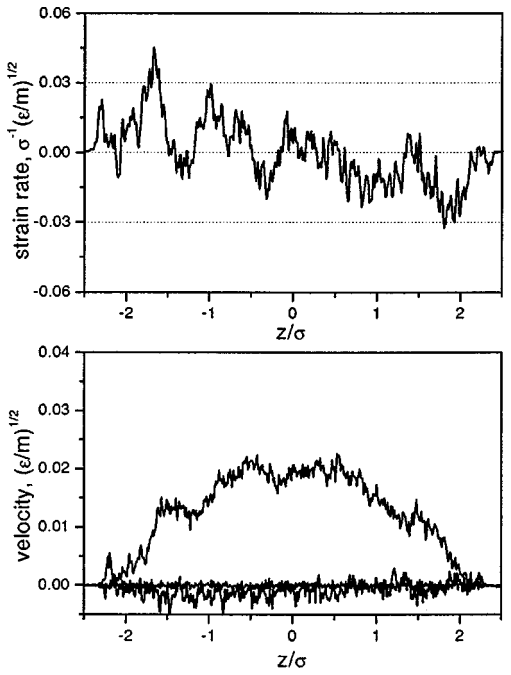

FIG. 15. The model WCA nanofluid: the NEMD velocity (bottom) and strain rate, $\partial u_x(z)/\partial z$, (top) profiles after 1 million EMD time steps for $n_{\mathrm{av}}^f=0.603$ and $T=0.958$. The bottom figure: the developed profile, $u_x(z)$; the two fluctuating lines parallel to the coordinate axis: low fluctuations, $u_y(z)$; large fluctuations, $u_z(z)$. Parameters: m, molecular mass; ε,σ, potential parameters.

attractive intermolecular interactions. At the lower average density the fluid-wall attractive intermolecular interactions lead to an increase in the LJ nanofluid average theoretical viscosity by 46% compared to that of the WCA nanofluid due to an increase in local ordering of the fluid molecules that manifests itself via an increase in the local density within the fluid layers and the corresponding contact values of the pair correlation functions. In bulk LJ fluids, when a fluid molecule moves it involves in the motion its neighborhood via attractive interactions of the molecules. These ''attractive'' correlations lead to a well known decrease by 30% in the viscosity of the bulk LJ fluid compared to that of the bulk WCA fluid at the same average density and temperature [21]. In the model LJ nanofluids this decrease is overrun by the increase in the viscosity due to the fluid-wall attractive intermolecular interactions. At the lower average density this increase in the viscosity of the LJ nanofluids compared to that of the WCA nanofluid is a phenomenon that does not have its counterpart for bulk fluids.

At the high average density the correlated motion of the well ordered layers of the LJ nanofluid ''help'' the LJ nanofluid to transform the shear stress into collective fluid motion, and therefore, lead to a decrease in the LJ nanofluid viscosity. When a LJ nanofluid layer moves it involves in the motion its neighboring layers via attractive interactions of the molecules in the neighboring layers. On the other hand, at high densities the fluid-wall attractive intermolecular interactions lead to increase in the viscosity of the model LJ nanofluid via an increase in the density and the contact values of the fluid-fluid pair correlation functions specific to the fluid layers near the walls. Similar to the case of the lowdensities, the decrease in the LJ nanofluid viscosity caused by the fluid-fluid attractive intermolecular interactions is largely exceeded by the increase in the LJ nanofluid viscosity due to the attractive interactions with the wall atoms. However, in the case of the high average density these alternative tendencies almost compensate each other. The calculated average PG viscosity of the model LJ nanofluid is about 14% lower than the average PG theoretical viscosity of the model WCA nanofluid. This deviation is within the statistical error of the viscosity calculations, and therefore, further sophisticated MD simulations are needed to recover the actual values of the PG theoretical viscosity of the model nanofluids at the high average density.

B. NEMD simulations: the velocity and density profiles, and heuristic viscosities

Our NEMD simulations of the Poiseuille flow of the model WCA and LJ nanofluids confirmed findings of Ref. [11] that for nanofluids confined in the pore of 5.1σ in width the streaming velocity profile differs from the parabolic one and possesses inflections that lead to oscillations of the corresponding strain rate profile. In our case of immobile wall atoms and small acting force $F_e=0.02$, the streaming velocity profiles became more structured and revealed more inflection regions than that of Ref. [11], where larger z bins, larger force value ($F_e=0.5$), and mobile wall atoms were used in the simulations. For both types of the nanofluids we performed 6 million time steps of the NEMD simulations to obtain steady and relatively smooth streaming velocity profiles (see Figs. 14–21) with fluctuations within the 15% range. According to our expectations, the flow of the model LJ fluid stabilizes faster than that of the model WCA fluid

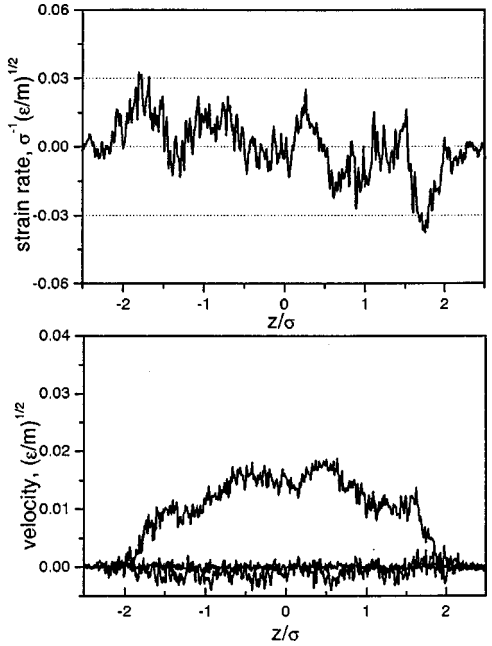

FIG. 16. The model LJ nanofluid: the NEMD velocity (bottom) and strain rate, $\partial u_x(z)/\partial z$, (top) profiles after 1 million EMD time steps for $n^f_{\rm av}=0.442$ and $T=0.729$. The bottom figure: the developed profile, $u_x(z)$; the two fluctuating lines parallel to the coordinate axis: low fluctuations, $u_y(z)$; large fluctuations, $u_z(z)$. Parameters: m, molecular mass; ε,σ, molecular paremeters.

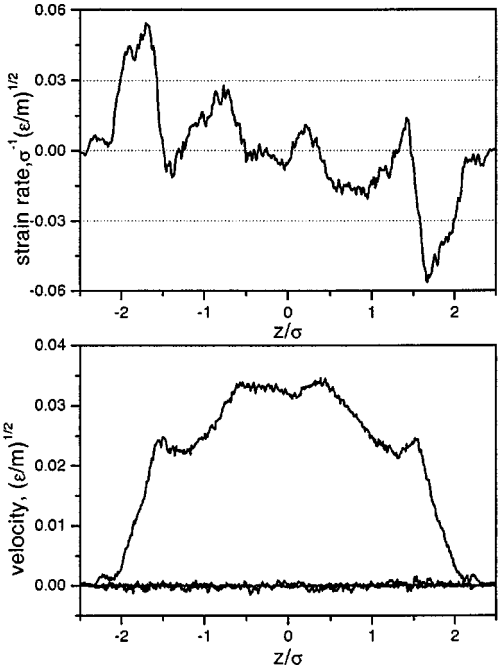

FIG. 18. The model WCA nanofluid: the NEMD velocity (bottom) and strain rate, $\partial u_x(z)/\partial z$, (top) profiles after 6 million EMD time steps for $n^f_{\rm av}=0.442$ and $T=0.729$. The bottom figure: the developed profile, $u_x(z)$; the two fluctuating lines parallel to the coordinate axis: low fluctuations, $u_y(z)$; large fluctuations, $u_z(z)$. Parameters; m, molecular mass; $\varepsilon\sigma$, potential parameters.

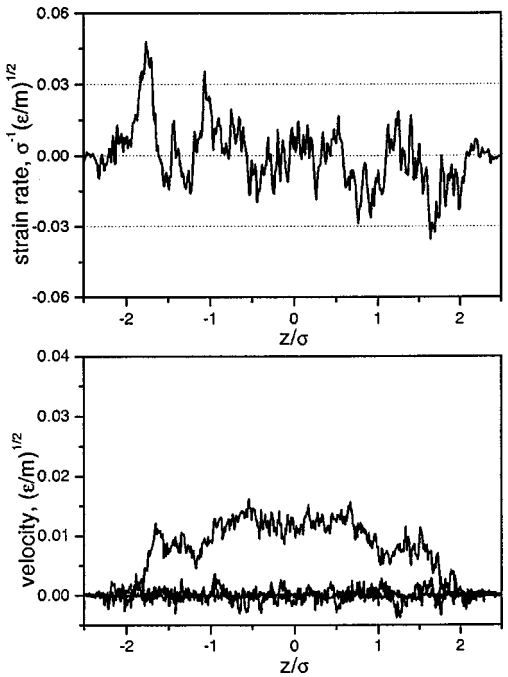

FIG. 17. The model LJ nanofluid: the NEMD velocity (bottom) and strain rate, $\partial u_x(z)/\partial z$, (top) profiles after 1 million EMD time steps for $n^f_{\rm av}=0.603$ and $T=0.958$. The bottom figure: the developed profile, $u_x(z)$; the two fluctuating lines parallel to the coordinate axis: low fluctuations, $u_y(z)$; large fluctuations, $u_z(z)$. Parameters: m, molecular mass; ε,σ, potential parameters.

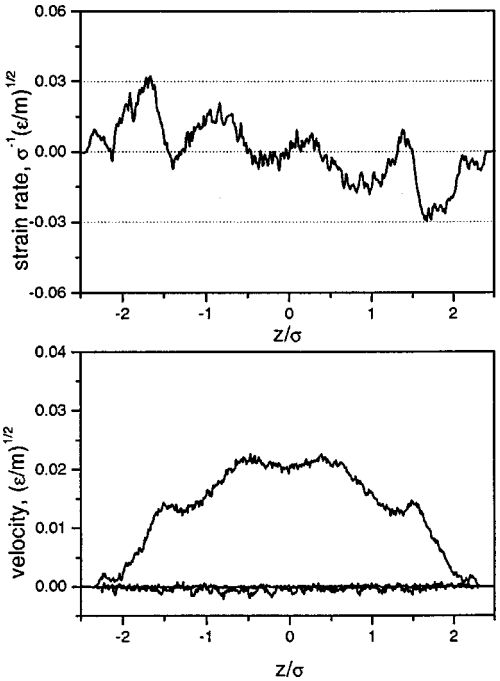

FIG. 19. The model WCA nanofluid: the NEMD velocity (bottom) and strain rate, $\partial u_x(z)/\partial z$, (top) profiles after 6 million EMD time steps for $n^f_{\rm av}=0.603$ and $T=0.958$. The bottom figure: the developed profile, $u_x(z)$; the two fluctuating lines parallel to the coordinate axis: low fluctuations, $u_y(z)$; large fluctuations, $u_z(z)$. Parameters: m, molecular mass; $\varepsilon\sigma$, potential parameters.

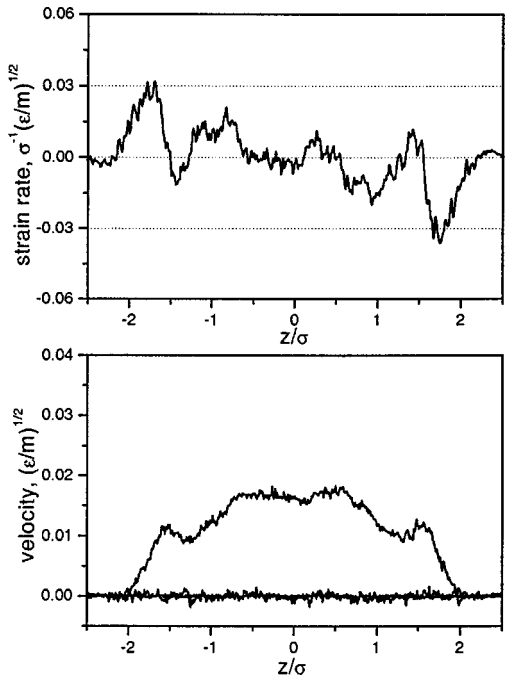

FIG. 20. The model LJ nanofluid: the NEMD velocity (bottom) and strain rate, $\partial u_x(z)/\partial z$, (top) profiles after 6 million EMD time steps for $n^f_{\rm av}=0.442$ and $T=0.729$. The bottom figure: the developed profile, $u_x(z)$; the two fluctuating lines parallel to the coordinate axis: low fluctuations, $u_y(z)$; large fluctuations, $u_z(z)$. Parameters: m, molecular mass; ε, σ, potential paramters.

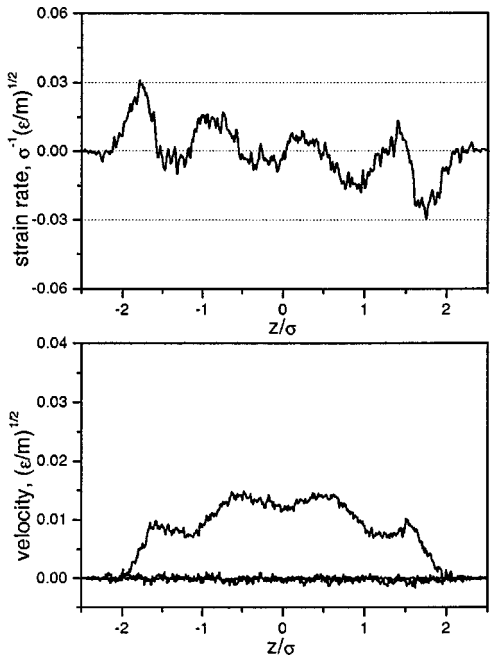

FIG. 21. The model LJ nanofluid: the NEMD velocity (bottom) and strain rate, $\partial u_x(z)/\partial z$, (top) profiles after 6 million EMD time steps for $n^f_{\rm av}=0.603$ and $T=0.958$. The bottom figure: the developed profile, $u_x(z)$; the two fluctuating lines parallel to the coordinate axis: low fluctuations, $u_y(z)$; large fluctuations, $u_z(z)$. Parameters: m, molecular mass; ε,σ, potential parameters.

due to the presence of the attractive interactions (compare, for example, the corresponding streaming velocity profiles after 1 million NEMD time steps shown in Figs. 14, 15 and 16, 17). At the lower average density all values of the streaming velocity of the LJ nanofluid flow are reduced by about 45% and the streaming velocity profile is flatter compared to those of the streaming velocity in the case of the model WCA nanofluid. This agrees quantitatively with the PG-theoretical prediction that the average viscosity of the model LJ nanofluid is larger by about 46% than that of the model WCA nanofluid at the lower average density (see Figs. 10 and 12). Therefore, we confirmed the prediction of the PG theory that in the case of nanofluids the effects of the fluid-wall attractive intermolecular interactions can significantly override effects caused by the fluid-fluid attractive intermolecular interactions and lead to about 45% increase in the viscosity of the model LJ nanofluid compared to that of the model WCA nanofluid at the same conditions, in contrast to the case of the corresponding bulk fluids.

In the case of high average density the streaming velocity profiles of the LJ and WCA nanofluids closely approach each other (the deviation in the average velocity values are about 20%). This means that the viscosity of the LJ nanofluid increases much slower with an increase in the average density than the viscosity of the WCA nanofluid, again confirming the tendency predicted by the PG transport theory (see Figs. 11 and 13). The average PG viscosity of the model LJ nanofluid at this density is 13% less than that of the WCA nanofluid. Noticing that this deviation is less than the error of the viscosity calculations in our EMD simulations, we conclude that the PG-theoretical average viscosities of the model LJ and WCA nanofluids practically coincide. However, the NEMD velocity profile specific to the LJ nanofluid is reduced by about 20% compared to that of the WCA nanofluid, and therefore, the LJ nanofluid viscosity, as reflected by the NEMD simulations, seems to be larger than that of the WCA nanofluid. We note here again, that our NEMD statistical error of the velocity profile computations (caused by the local velocity fluctuations) was about 15% after 6 million NEMD time steps. Therefore, the NEMD streaming velocity profile at the high average density lies almost within the ''experimental'' error from that of the WCA nanofluid. We also note that relaxation processes in the model WCA nanofluid are much slower than those in the model LJ fluid at the same conditions, and therefore, further simulations for additional several million NEMD time steps may be needed to observe the same steady state of the WCA nanofluid as that of the LJ one after 6 million time steps.

Numerical evaluation of the heuristic expressions (4.4), (4.5), (4.6), (4.7), (4.8), and (4.9) confirmed that only two of them, $\eta_{p\text{-av}}$ and $\eta_{\rm total}$ of Eqs. (4.5) and (4.6), respectively, can supply physically meaningful values of the nanofluid viscosity. These values are shown in Figs. 10–13 and can be used for rough evaluation of the average viscosity of the studied model nanofluids ''from beneath'' ($\eta_{p\text{-av}}$) and ''from above'' ($\eta_{\rm total}$) fairly successfully. For three case studies out of a total of four the average PG theoretical viscosity lies between the corresponding $\eta_{p\text{-av}}$ and $\eta_{\rm total}$ values. However, in the case of the WCA nanofluid at the high density $\eta_{\rm total}$ fails to supply the proper upper bound, and also the value of $\eta_{p\text{-av}}$ is too low to be considered as a reasonable lower bound (see Fig. 11). This indicates that heuristic expressions (4.5) and (4.6) are likely to fail at high densities. We demonstrate below, that such a failure is typical for empirical formulas

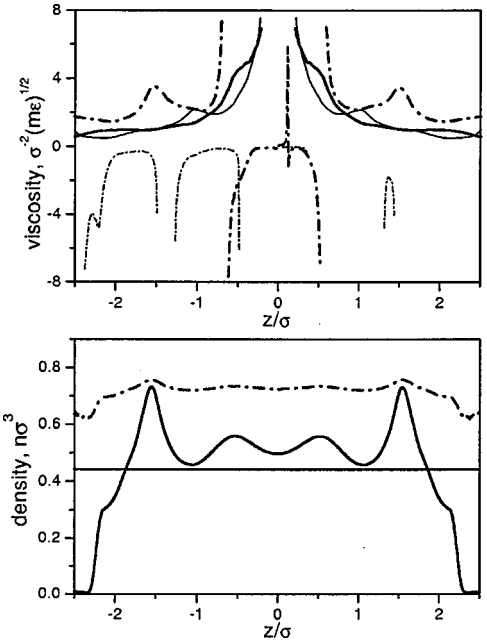

FIG. 22. The NEMD simulations: the profiles of the heuristic viscosities (top) and number density of the WCA nanofluid after 6 million NEMD time steps for $n^f_{\rm av}=0.442$ and $T=0.729$. The top figure: (1) thin dash-dot curves, $\eta_{\rm IMC}(z)$; (2) thick dash-dot curves, $\eta_{{\rm IMC}\,f}(z)$; (3) thick solid curves, $\eta_\sigma(z)$; (4) thin solid curves, $\eta_{\sigma/2}(z)$. The bottom figure: (1) solid curve, the number density; (2) dash-dot curve, temperature. Parameters: m, molecular mass; ε,σ, potential parameters.

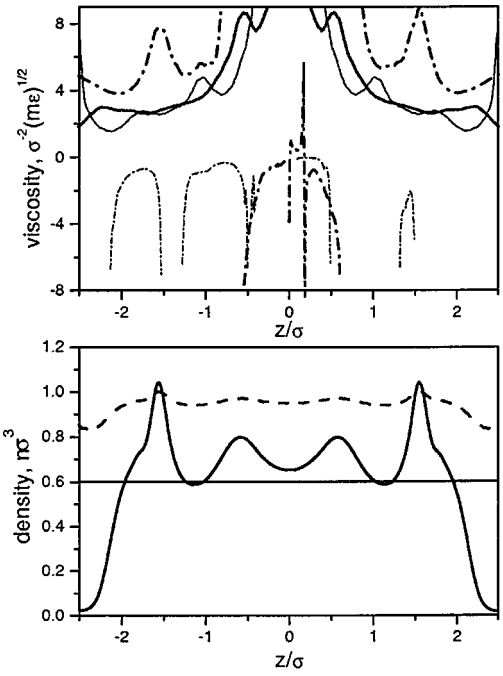

FIG. 23. The NEMD simulations: the profiles of the heuristic viscosities (top) and number density of the WCA nanofluid after 6 million NEMD time steps for $n^f_{\rm av}=0.603$ and $T=0.958$. The top figure: (1) thin dash-dot curves, $\eta_{\rm IMC}(z)$; (2) thick dash-dot curves, $\eta_{{\rm IMC}\,f}(z)$; (3) thick solid curves, $\eta_\sigma(z)$; (4) thin solid curves, $\eta_{\sigma/2}(z)$. The bottom figure: (1) solid curve, the number density; (2) dash-dot curve, temperature. Parameters: m, molecular mass; ε,σ, potential parameters.

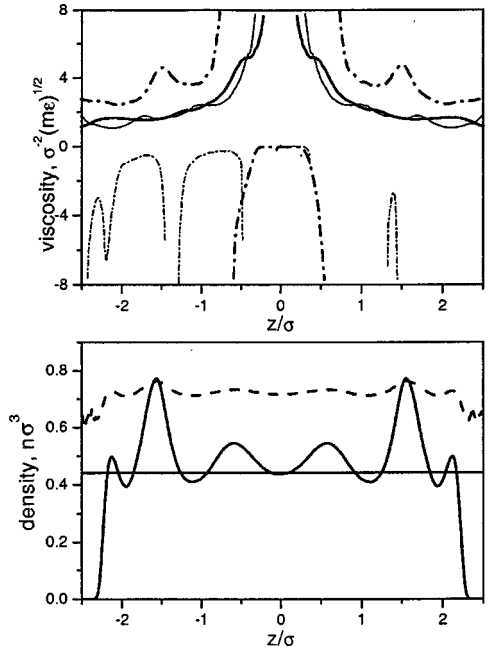

FIG. 24. The NEMD simulations: the profiles of the heuristic viscosities (top) and number density of the LJ nanofluid after 6 million NEMD time steps for $n^f_{\rm av}=0.442$ and $T=0.729$. The top figure: (1) thin dash-dot curves, $\eta_{\rm IMC}(z)$; (2) thick dash-dot curves, $\eta_{{\rm IMC}\,f}(z)$; (3) thick solid curves, $\eta_\sigma(z)$; (4) thin solid curves, $\eta_{\sigma/2}(z)$. The bottom figure: (1) solid curve, the number density; (2) dash-dot curve, temperature. Parameters: m, molecular mass; ε,σ, potential parameters.

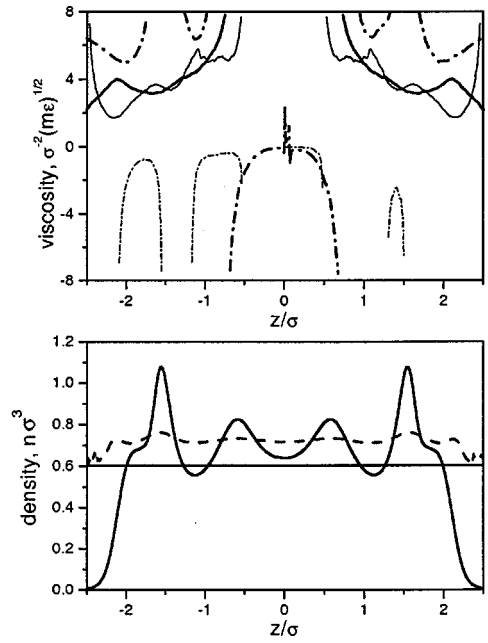

FIG. 25. The NEMD simulations: the profiles of the heuristic viscosities (top) and number density of the LJ nanofluid after 6 million NEMD time steps for $n^f_{\rm av}=0.603$ and $T=0.958$. The top figure: (1) thin dash-dot curves, $\eta_{\rm IMC}(z)$; (2) thick dash-dot curves, $\eta_{{\rm IMC}\,f}(z)$; (3) thick solid curves, $\eta_\sigma(z)$; (4) thin solid curves, $\eta_{\sigma/2}(z)$. The bottom figure: (1) solid curve, the number density; (2) dash-dot curve, temperature. Parameters: m, molecular mass; ε,σ, potential parameters.

that do not incorporate details of the nanofluid structure.

The results of our calculations of the heuristics viscosities defined by Eqs. (4.4), (4.7), (4.8), and (4.9) are shown in Figs. 22–25. Due to the oscillations of the strain rate profiles the quantity η_{IMC} fails badly everywhere within the pore supplying unphysical (negative and divergent) numerical values of the nanofluid viscosity for all the case studies. The other three quantities $\eta_{\sigma}, \eta_{\sigma/2}$, and $\eta_{\mathrm{IMC}f}$, are divergent in the pore center due to the symmetry of the velocity profile.

The NEMD temperature and density profiles recovered in the NEMD simulations are shown in Figs. 22–25. While the temperature was constant within the pore space, it was lower by about 14% next to the wall surface atoms, because of an increase in statistical errors due to the low density of the fluids at positions less than $\sigma/2$ from the pore walls. The NEMD density profiles for all the case studies are almost identical in the shape and magnitude to those obtained in the EMD simulations (the deviations do not exceed 7%). This again confirms a well known fact that the laminar flow does not affect the equilibrium structure of nanofluids.

VI. CONCLUSIONS

In this study we calculated the viscosity of the model WCA and LJ nanofluids using the simplified formula, Eq. (2.3), of the PG transport theory of inhomogeneous fluids and a number of heuristic expressions. We proved that the simplified PG expression supplies numerically reasonable and physically meaningful values of the model nanofluid viscosities in all the case studies, while *all the heuristic expressions fail*. This result is supported by the conclusions drawn upon analysis of the streaming velocity profiles of the Poiseuille flow of the model nanofluids recovered in the process of the NEMD simulations. The PG theoretical viscosity supplies a quantitatively accurate description of the flow properties and reflects major tendencies in the flow behavior. Unfortunately, due to the nature of the simulation methods, the NEMD simulations cannot provide actual values of the transport coefficients of fluids by means other than the use of heuristic formulas similar to those of Eqs. (4.4)–(4.9). Unless another development of a rigorous statistical mechanical theory similar to the PG theory is undertaken, such formulas are bound to involve intuitive considerations that are built upon the knowledge gained mainly from the studies of the transport behavior of homogeneous or weakly inhomogeneous fluids. Such fluids are macroscopically isotropic, and therefore, the contributions into the transport properties of such fluids that are due to the fluid structure factors (i.e., the number density and correlation functions) are ''smoothed.'' This means that for such fluids the details of the local fluid structure are not manifested dramatically in the fluid transport properties.

Contrary to the case of the weakly inhomogeneous fluids, for dense, strongly inhomogeneous fluids and nanofluids in particular, the dramatical variations in the fluid structure factors over the length scale comparable to the fluid particle dimensions can lead to a dramatical change in the fluid transport properties of such fluids compared to those of the corresponding bulk fluids. The major contributions due to the fluid structure come into the fluid transport properties via the number density and pair correlation functions, and therefore, any physically meaningful expression for transport coefficients of such fluids has to incorporate the information on the fluid number density and pair correlation functions, at the very least. A strong feature of the PG transport theory is that in this theory the transport coefficients of inhomogeneous fluids are expressed in terms of the *equilibrium* structure factors, and therefore, are well-defined and can be easily calculated.

In the case of nanosystems (i.e., systems composed of a small number of molecules within the space dimensions comparable to those of the system particles) the physical meaning of the description of the systems properties in terms of the collective modes changes. For such systems this description does not supply ''macroscopic'' physical properties; rather, it supplies probabilistic, expectation values of such properties. The average, physically measurable transport coefficients are further supplied by averaging of such expectation values over appropriate subsystems of the nanosystem.

In the context of the viscosity calculations this means in particular, that the PG theoretical expression, Eq. (2.3), supplies the expectation values of the local nanofluid viscosity in a slit pore. When the pore is of several molecular diameters in width the position dependence of the confined fluid viscosity cannot be measured directly; rather, one can measure the average pore viscosity, and then compare the results with those obtained by averaging the expression for the local PG viscosity over the pore cross-section. When the system size grows the theoretical expectation values approach the measurable average values. For studied nanofluid systems this happens when the pore width exceeds ten molecular diameters [10,11]. For such wider pores the PG expressions for transport coefficients reduce [8] to those of the bulk fluids [21].

In our simulation studies we recovered the contact values of the pair correlation functions of the model nanofluids within the statistical error of about 20%, and the PG theoretical viscosity and the streaming velocity profiles within the statistical error of about 15%. Further simulation studies are needed to reduce these errors and also to consider applications of the PG transport theory to other types of nanofluid systems. Such studies are planned for the near future.

ACKNOWLEDGMENTS

The author thanks K. E. Gubbins for useful discussions, and E. Kontar and Ya. Tkach for technical assistance and system support. This research was supported by a grant from the Civilian Research and Development Foundation.

[1] S.-T. Hwang and K. Kammermeyer, *Membranes in Separation* (Wiley, New York, 1975).

[2] K.J. Mysels and M.C. Cox, J. Colloid Sci. **17**, 136 (1962); J. Lyklema, P.C. Scholten, and K.J. Mysels, J. Phys. Chem. **69**, 116 (1965),

[3] B.V. Derjaguin, Chem. Scr. **9**, 97 (1976); B.V. Derjaguin,

Ya.I. Rabinovich, and N.V. Churaev, Nature (London) **272**, 313 (1978).

[4] See, for example, Ya.I. Rabinovich, B.V. Derjaguin, and Yu.P. Toporov, J. Colloid Sci. **7**, 251 (1983); D.Y.C. Chan and R.G. Horn, J. Chem. Phys. **83**, 5311 (1985); J.N. Israelachvili, J. Colloid Sci. **110**, 263 (1986); J.N. Israelachvili, P.M. McGuiggan, and A.M. Homola, Science **240**, 189 (1988); M.L. Gee, P.M. McGuiggan, and J.N. Israelachvili, J. Chem. Phys. **93**, 1 (1990); J. Van Alsten and S. Granick, Phys. Rev. Lett. **61**, 2570 (1998); J. Van Alsten and S. Granick, Langmuir **6**, 976 (1990); S. Granick, Science **253**, 1374 (1991).

[5] S. Toxvaerd, J. Chem. Phys. **74**, 1998 (1981); M. Schoen, D.J. Diestler, and J.H. Cushman, *ibid.* **87**, 5464 (1987); D.J. Diestler, M. Schoen, A.W. Hertzner, and J.H. Cushman, *ibid.* **95**, 5432 (1991); I. Bitsanis, J.J. Magda, M. Tirrell, and H.T. Davis, *ibid.* **87**, 1733 (1987); J.J. Magda, M. Tirrell, and H.T. Davis, *ibid.* **88**, 1207 (1988); I. Bitsanis, S.A. Somers, H.T. Davis, and M. Tirrell, *ibid.* **93**, 3427 (1990); S.-H. Suh and J.M.D. MacElroy, Mol. Phys. **58**, 445 (1986); J.M.D. MacElroy and S.-H. Suh, *ibid.* **60**, 475 (1987).

[6] I. Bitsanis, T.K. Vanderlick, M. Tirrell, and H.T. Davis, J. Chem. Phys. **89**, 3152 (1988).

[7] H.T. Davis, J. Chem. Phys. **86**, 1474 (1987); Chem. Eng. Commun. **58**, 413 (1987).

[8] L.A. Pozhar and K.E. Gubbins, J. Chem. Phys. **99**, 8970 (1993); L.A. Pozhar and K.E. Gubbins, Phys. Rev. E **56**, 5367 (1997); L.A. Pozhar, *Transport Theory of Inhomogeneous Fluids* (World Scientific, Singapore, 1994); L.A. Pozhar and K.E. Gubbins, Int. J. Thermophys. **20**, 805 (1999).

[9] L.A. Pozhar, Ukr. Phys. J. **34**, 779 (1989) (in Russian); L.A. Pozhar and K.E. Gubbins, J. Chem. Phys. **94**, 1367 (1991).

[10] E. Akhmatskaya, B.D. Todd, P.J. Daivis, D.J. Evans, K.E. Gubbins, and L.A. Pozhar, J. Chem. Phys. **106**, 4684 (1997).

[11] K.P. Travis, B.D. Todd, and D.J. Evans, Physica A **240**, 315 (1997).

[12] B.D. Todd, D.J. Evans, and P.J. Davis, Phys. Rev. E **52**, 1627 (1995); see also S. Sarman, D.J. Evans, and P.T. Cummings, Phys. Rep. **305**, 1 (1998), for further references and discussion of such algorithms.

[13] J.A. Barker and D. Henderson, J. Chem. Phys. **47**, 4714 (1967).

[14] J.D. Weeks, D. Chandler, and H.C. Andersen, J. Chem. Phys. **54**, 5237 (1971).

[15] M.P. Allen and D.J. Tildesley, *Computer Simulation of Liquids* (Clarendon, Oxford, 1987).

[16] C.G. Gray and K.E. Gubbins, *Theory of Molecular Fluids. I. Fundamentals* (Clarendon, Oxford, 1984), Chap V.

[17] J.L. Buchanan and P.R. Tumer, *Numerical Methods and Analysis* (McGraw-Hill, New York, 1992).

[18] B.D. Todd and D.J. Evans, J. Chem. Phys. **103**, 9804 (1995).

[19] J.H. Fertziger and H.G. Kaper, *Mathematical Theory of Transport Processes in Gases* (North-Holland, New York, 1972); J.O. Hirschfelder, C.F. Curtiss, and R.B. Bird, *Molecular Theory of Gases and Liquids* (Wiley, New York, 1954).

[20] J. Van Alsten and S. Granick, Tribol. Trans. **32**, 246 (1989); H.-W. Hu, G.A. Carson, and S. Granick, Phys. Rev. Lett. **66**, 2758 (1991).

[21] W. Sung and J.S. Dahler, J. Chem. Phys. **80**, 3025 (1984).